Extracellular vesicles from human pancreatic islets suppress human islet amyloid polypeptide amyloid formation

Diana Ribeiro[a,b], Istvan Horvath[b], Nikki Heath[c], Ryan Hicks[a], Anna Forslöw[a], and Pernilla Wittung-Stafshede[b,1]

[a]Discovery Biology, Innovative Medicines and Early Development Biotech Unit, AstraZeneca, 43150 Mölndal, Sweden; [b]Department of Biology and Biological Engineering, Chalmers University of Technology, 41258 Gothenburg, Sweden; and [c]Discovery Biology, Innovative Medicines and Early Development Biotech Unit, AstraZeneca, Alderley Park SK10 4TG, United Kingdom

Edited by Alan R. Fersht, Medical Research Council Laboratory of Molecular Biology, Cambridge, United Kingdom, and approved September 11, 2017 (received for review June 28, 2017)

Extracellular vesicles (EVs) are small vesicles released by cells to aid cell–cell communication and tissue homeostasis. Human islet amyloid polypeptide (IAPP) is the major component of amyloid deposits found in pancreatic islets of patients with type 2 diabetes (T2D). IAPP is secreted in conjunction with insulin from pancreatic β cells to regulate glucose metabolism. Here, using a combination of analytical and biophysical methods in vitro, we tested whether EVs isolated from pancreatic islets of healthy patients and patients with T2D modulate IAPP amyloid formation. We discovered that pancreatic EVs from healthy patients reduce IAPP amyloid formation by peptide scavenging, but T2D pancreatic and human serum EVs have no effect. In accordance with these differential effects, the insulin: C-peptide ratio and lipid composition differ between EVs from healthy pancreas and EVs from T2D pancreas and serum. It appears that healthy pancreatic EVs limit IAPP amyloid formation via direct binding as a tissue-specific control mechanism.

extracellular vesicles | type 2 diabetes | amyloid | atomic force microscopy | electron microscopy

Type 2 diabetes (T2D) is becoming increasingly common worldwide, due in part to the rise in obesity (1). Like many neurodegenerative disorders, such as Parkinson's and Alzheimer's diseases, as well as various systemic amyloidosis conditions, T2D is a protein-misfolding disease involving aberrant amyloid fiber formation (2). The primary pathological characteristic of T2D is islet amyloid of the hormone amylin, also known as islet amyloid polypeptide (IAPP), in pancreatic β cells (3–6). The process of islet amyloid formation (7–9) leads to pancreatic β-cell dysfunction, followed by cell death. In T2D, compromised β-cell function causes a gradual loss of β-cell mass, which impairs insulin (INS) secretion (10, 11). IAPP is cosecreted with INS after enzymatic maturation of prohormones pro-IAPP and proinsulin in secretory granules (12). IAPP and INS have roles in controlling gastric emptying and glucose homeostasis and in suppressing glucagon release. Although not understood on a mechanistic level, impairment of prohormone processing is thought to play a role in the initiation and progression of T2D (13, 14).

Virtually all cells in an organism secrete extracellular vesicles (EVs), a heterogeneous population of membrane-enclosed vesicles that transport and deliver payloads of proteins and nucleic acids to recipient cells (15, 16). The protein, nucleic acid, and lipid contents of EVs vary depending on the source cell, and the contents of EVs from different cell types have been characterized (www.microvesicles.org; www.exocarta.org). In recent years, research into EVs has expanded dramatically with a major focus on exosomes, defined by their size and the presence of various protein and nucleic acid markers (17). Exosomes are ∼100 nm in diameter, of endosomal origin, and facilitate intercellular communication. Exosomes have been shown to regulate many pathophysiological processes, including immune response, inflammation, and infection (18, 19), but their roles in metabolic diseases have not been well explored (20). Pancreatic islets and β cells also secrete EVs, which have been found to regulate local and systemic responses to β-cell stress (21) and to transfer cargo to, for example, phagocytes (22). Moreover, EVs from pancreatic cancer cells appear to play a role in autoimmunity (23) and β-cell dysfunction (24), and to possibly act as disease biomarkers (18, 19). Analysis of the mRNA content of EVs secreted from human pancreatic islets has suggested a putative role in β-cell–endothelium cross-talk and neoangiogenesis (25). It may be speculated that EVs derived from pancreatic islets of patients with TD2 (compared with EVs from islets of healthy donors) may reflect phenotypic changes occurring in the β cells during disease development.

Even with a few recent reports, the roles of EVs, such as exosomes, in amyloid diseases remain mostly unexplored. Exosomes from neuroblastoma cells were found to accelerate amyloid formation of the Parkinson's disease protein α-synuclein in vitro via a process that depends on certain ganglioside lipids in the neuronal exosomes (26). Neuron-derived exosomes have been found to promote amyloid β peptides to form nontoxic amyloids, which are internalized by microglia and then transported to lysosomes for degradation (27). EVs also have been shown to transport amyloidogenic proteins and amyloid fiber seeds or oligomers from cell to cell, potentially causing a prion-like spread of disease (18, 19, 28). Cerebrospinal fluid exosomes

Significance

Protein assembly into amyloid fibers underlies such neurodegenerative disorders as Alzheimer's disease and Parkinson's disease. Type 2 diabetes (T2D) also involves amyloid formation, although in the pancreas. Because there are no cures for amyloid diseases and T2D is on the rise due to an increasing prevalence of obesity, identifying involved mechanisms and control processes is of utmost importance. Extracellular vesicles (EVs) can mediate physiological and pathological communication both locally and at a distance. Here, we demonstrate that EVs secreted from healthy, but not from T2D, pancreatic cells slow amyloid formation of the major peptide found in amyloid deposits in T2D. We propose an EV-mediated process that tempers amyloid formation in the pancreas at normal conditions, which breaks down in T2D due to altered EV protein–lipid composition.

Author contributions: D.R., I.H., N.H., R.H., A.F., and P.W.-S. designed research; D.R. and I.H. performed research; D.R., I.H., N.H., and R.H. contributed new reagents/analytic tools; D.R., I.H., N.H., R.H., A.F., and P.W.-S. analyzed data; and P.W.-S. wrote the paper.

The authors declare no conflict of interest.

This article is a PNAS Direct Submission.

Freely available online through the PNAS open access option.

[1]To whom correspondence should be addressed. Email: pernilla.wittung@chalmers.se.

This article contains supporting information online at www.pnas.org/lookup/suppl/doi:10.1073/pnas.1711389114/-/DCSupplemental.

from patients with Parkinson's disease have been found to contain α-synuclein species that readily induce aggregation of α-synculein in a reporter cell line (29). Investigations of the putative effects on IAPP amyloid formation by EVs secreted from pancreatic islets in the context of T2D are lacking, however. Since IAPP amyloid formation is affected by synthetic lipid vesicles in vitro (8, 30–32), EVs may be predicted to have effects as well. To begin to address this question, we isolated and characterized EVs from pancreatic islets of healthy patients and patients with T2D, and investigated the effects of these EVs on IAPP amyloid formation in vitro.

Results and Discussion

Characterization of Human Islet EVs. EVs were collected from cultures of human pancreatic islets from healthy patients and patients with T2D, which contained a mean of 1,500 ± 433 and 1,900 ± 630 islets/mL, respectively (*SI Appendix*, Table S1). In addition to EVs from healthy and diabetic pancreatic islets, we also included EVs isolated from human serum as control EVs. Analysis of total protein content (Fig. 1*A*) and total particle content (Fig. 1*B*) revealed similar concentrations in all three EV samples (i.e., ∼5 mg/mL protein; 5–10 nM EVs). The size distribution of the EVs was characterized by nanoparticle tracking analysis (NTA) (Fig. 1*C*), which showed the control serum EVs to be the largest (∼105 nm) and the healthy pancreas EVs to be the smallest (∼95 nm), but overall all EVs showed a size distribution of ∼100 nm in diameter, a value typically associated with exosomes (17). The measured ζ potentials for the EVs were all negative and did not vary among the three types (Fig. 1*D*). The values obtained were in the same range as those for small unilamellar vesicles made with anionic lipids (26). A comparison of ζ potentials between pancreatic EVs and exosomes from neuronal cells (26) showed that pancreatic EVs are less negatively charged (−7 mV vs. −16 mV).

To get an idea about the cargo of the EVs, we analyzed protein content by ELISA. In related work, we have established that the pancreatic EVs contain many typical markers of exosomes, probed at both mRNA and protein levels. Here, we quantified the content of INS, C-peptide (C-PEP; the C-terminal part of the pro-INS peptide, cleaved off when mature INS is produced; ref. 12), and IAPP in the three types of EVs studied (Fig. 1 *D*–*F*). We found the EVs from healthy islets to have approximately fivefold less INS than C-PEP, whereas for T2D EVs and serum EVs, the amounts of INS and C-PEP were roughly equal. Notably, the absolute amount of C-PEP was lower in T2D and serum-derived

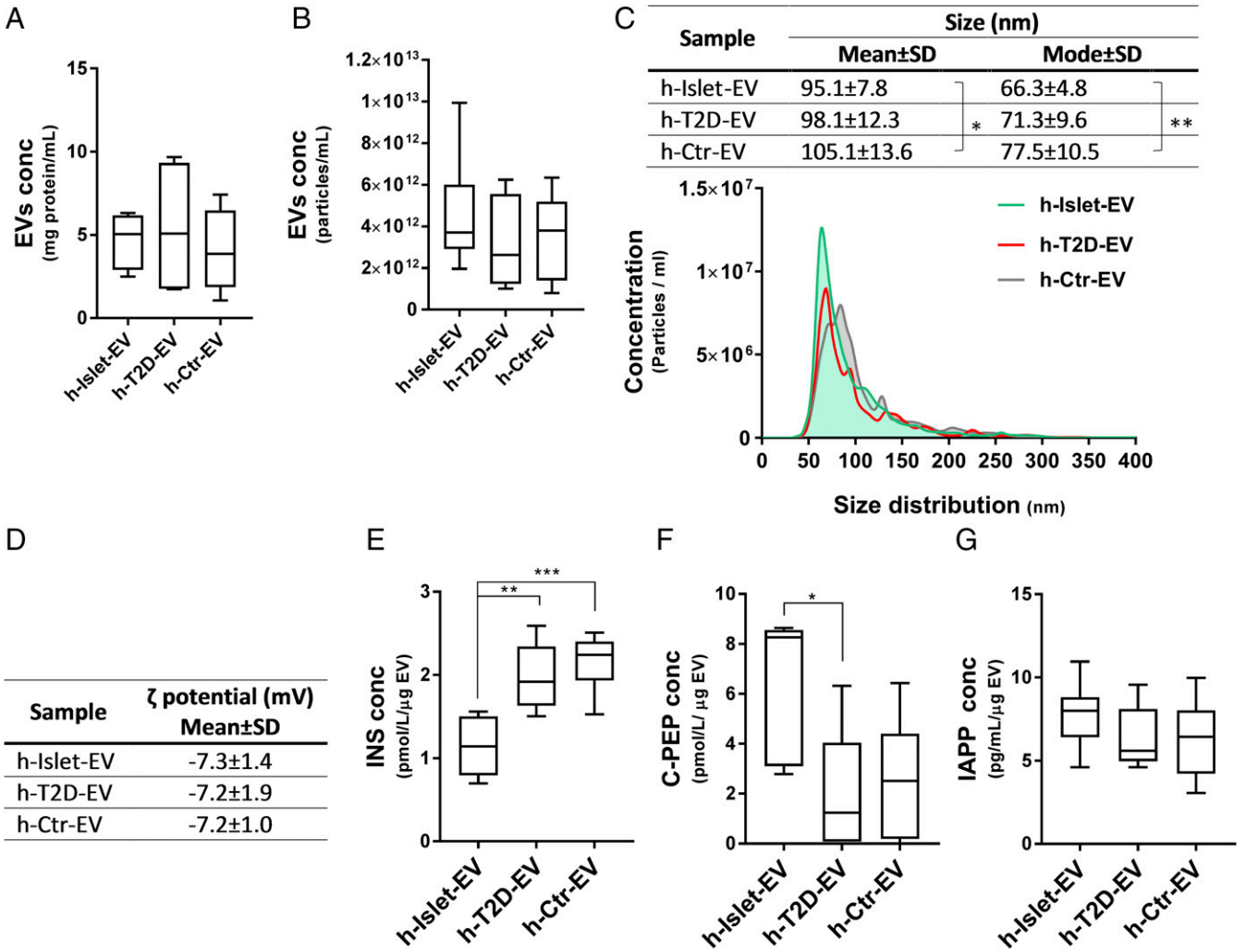

Fig. 1. Human pancreatic islet EV characterization. EVs were isolated from cultures of 10 mL of nondiabetic islets donors (h-Islet-EVs), islets from diabetic donors (h-T2D-EVs), and human serum from culture medium (h-Ctr-EVs). EVs were characterized by total protein concentration (*A*), particle concentration (*B*), size distribution (*C*), ζ potential (*D*), and human pancreatic hormones INS (*E*), C-PEP (*F*), and IAPP (*G*) as measured by ELISA. *, **, and *** represent statistical significance: *$P < 0.05$; **$P < 0.01$; ***$P < 0.001$.

EVs than in EVs from healthy islets, but IAPP amounts were similar in all three EV types. Less INS than C-PEP matches with the lower stability of INS (vs. C-PEP) in vivo, resulting in fivefold less INS compared with C-PEP in systemic circulation under normal conditions (33). Because C-PEP appears to be the best indicator of INS production, the lower levels of C-PEP in T2D EVs may reflect lower INS production. Nonetheless, how the peptide levels inside EVs relate to the amounts circulating in the body is not clear. Despite the lack of a molecular explanation, these results demonstrate divergent C-PEP content between healthy and T2D pancreatic EVs.

EV Effects on IAPP Amyloid Formation. We next assessed IAPP amyloid formation as a function of EV additions. For this, we used thioflavin T (ThT) fluorescence to monitor amyloid formation, as is commonly used in in vitro amyloid experiments (34, 35). IAPP alone is aggregation-prone and forms amyloids within 5–10 min under the conditions used here (Fig. 2*A*). When EVs from healthy islets were added, a concentration-dependent (using EV protein content as the measure, which is proportional to the number of EVs) decrease in ThT fluorescence was detected (Fig. 2*A*). Analysis of fluorescence at 10 min as a measure of reaction extent demonstrated significantly reduced amyloid formation at the highest EV concentration used, 25 μg/mL of EV protein (corresponding to ∼0.05 nM EVs) (Fig. 2*B*).

To assess whether the EVs themselves were responsible for the retarding effects on IAPP amyloid formation, we filtered the EVs and tested the EV-free solution in IAPP aggregation reactions (*SI Appendix*, Fig. S1*A*). No effect of the EV-free solution on IAPP amyloid formation was detected, implying that it is indeed the EVs (specific lipids or membrane-protruding proteins) that mediate the effect. As a control, we added BSA in the same amount as the EV protein content (25 μg/mL), and found no effect on IAPP amyloid formation (*SI Appendix*, Fig. S1*A*). We note that EVs alone had no effect on ThT fluorescence (*SI Appendix*, Fig. S1*B*), and when EVs were added to preaggregated IAPP (i.e., after a 20-min incubation), no reduction of the ThT intensity was detected (*SI Appendix*, Fig. S1*C*). Thus, the EVs do not dissolve preformed IAPP amyloid fibers.

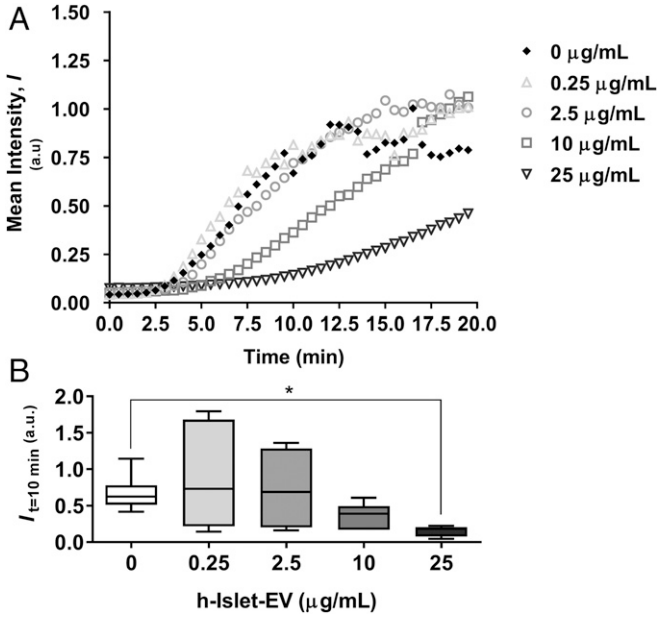

Fig. 2. Concentration-dependent effect of h-Islet-EVs on h-IAPP aggregation. (*A*) ThT fluorescence assay over time (min). (*B*) Mean intensity at 10 min of incubation. *Statistical significance compared with 0 μg/mL EVs: $P < 0.05$.

To directly compare EVs from healthy and T2D islets as well as human serum EVs, we added all three types to IAPP aggregation experiments at a concentration of 25 μg/mL (Fig. 3*A*). The ThT assay showed a significant retardation of amyloid formation in the healthy EVs, as confirmed in Fig. 2*B*. TEM analysis of the resulting products revealed that in contrast to IAPP alone, in which typical amyloid fibers were readily observed, no amyloid fibers were detected in IAPP mixed with healthy pancreatic EVs (Fig. 3*C*). Instead, some amorphous aggregates were visible in the images that may be EVs alone or EVs with IAPP. When T2D and serum EVs were added to IAPP aggregation reactions, no significant effects on IAPP amyloid formation were detected (Fig. 3*B*) and amyloid fibers were clearly detected by TEM (Fig. 3*C*), although they appeared "fuzzy," implying that EV fragments may attach to the IAPP amyloids.

To test the amyloid-reducing effect of the EVs from pancreatic islets on another aggregation-prone polypeptide, we turned to α-synuclein. The 140-residue α-synuclein is the amyloidogenic protein in Parkinson's disease and the major component of Lewy bodies found in brains of patients with Parkinson's disease (36–38), but also can be found in the pancreas (39). We recently showed that IAPP monomers and IAPP amyloid fibers can exaggerate α-synuclein amyloid formation in vitro, suggesting a possible explanation for why individuals with T2D are prone to Parkinson's disease (40). Interestingly, as probed by ThT fluorescence and atomic force microscopy (AFM), EVs from both healthy and T2D islets reduced α-synuclein amyloid formation when added at the same EV:protein ratio as in the IAPP experiments (*SI Appendix*, Fig. S2). This is a reasonable result, given that several types of negatively charged synthetic lipid vesicles can bind α-synuclein and modulate amyloid formation (41).

Mechanistic Insights into EV-Mediated IAPP Amyloid Inhibition. To address how healthy pancreatic EVs inhibit IAPP amyloid formation, we probed the mixtures using size exclusion chromatography (SEC). Freshly dissolved IAPP elutes as a monomer (Fig. 4*A*), whereas EVs are large enough to elute in the void of the SEC column but are not filtered away in the 0.2-μm precolumn filter (Fig. 4*B*). AFM of the EV fraction showed the presence of nanosized vesicles (Fig. 4*B*), in accordance with the NTA data. When IAPP and EVs were freshly mixed together and immediately eluted, no reaction was apparent, with the elution profile matching the sum of the individual samples described above (Fig. 4*C*). Incubation of IAPP resulted in amyloid fibers, which were filtered away before injection into the column, with no absorption at 280 nm detected on SEC (Fig. 4*D*). However, for an incubated mixture of IAPP and healthy islet EVs that showed no increase in ThT fluorescence or amyloid fibers by TEM, no monomeric IAPP was detected by SEC, and absorption of the EVs in the void was reduced (Fig. 4*D*, arrow). This suggests that IAPP binds to the EVs, resulting in larger particles, some of which are filtered away before SEC analysis, as well as the absence of monomeric IAPP. This result is not direct proof of an IAPP–EV interaction, however. Nonetheless, in agreement with the conclusion based on the SEC analysis, AFM showed that the EVs appeared larger in the presence of IAPP (Fig. 4*E*). The larger EVs can be explained either by IAPP-induced fusion of several EVs or by surface binding of many IAPP peptides per EV.

We also analyzed the lipid composition of the EVs using the HPLC-charged aerosol detection (CAD) technique (Fig. 5 and *SI Appendix*, Fig. S4). Six classes of lipids were detected and could be quantified: steryl ester (SE), triacylglycerol (TAG), cholesterol (CH), phosphatidylethanolamine (PE), sphingomyelin (SM), and phosphatidylcholine (PC). We also searched for free fatty acids, cardiolipin, phosphatic acid,

BIOCHEMISTRY

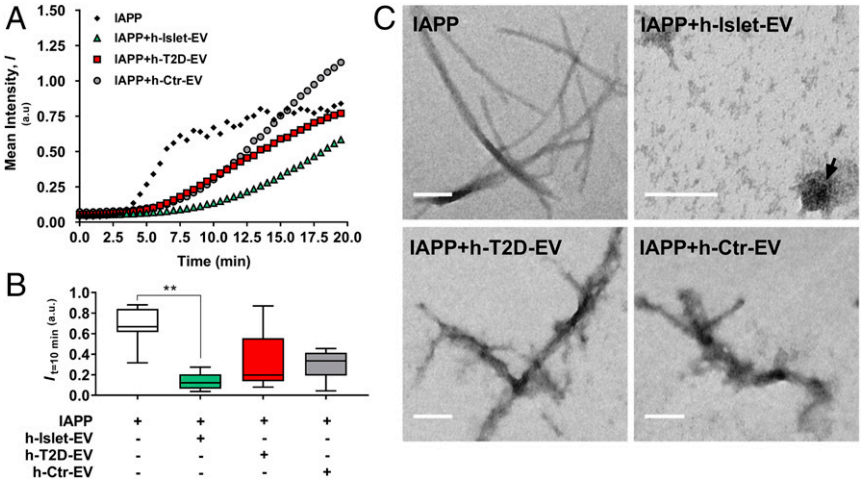

Fig. 3. Aggregation of IAPP in the presence of different EV populations. (*A*) ThT fluorescence assay over time (min). (*B*) mean ThT intensity at 10 min of incubation. **Statistical significance compared with 0 μg/mL EVs: $P < 0.01$. (*C*) TEM imaging of typical fibrils formed. (Scale bar: 100 nm.) The arrow points to an intact EV.

phosphatidylserine, and phosphatidylinositol, but did not detect these molecules in our samples. A comparison of the lipid contents in the three different EV samples showed different lipid profiles in serum EVs and pancreatic EVs (Fig. 5*A*), as could be expected. Although no significant differences between healthy and T2D pancreatic EVs were found on two-way ANOVA (*SI Appendix*, Fig. S3), this analysis suggested that healthy EVs have slightly higher CH, PC, and SM levels (at the expense of TAG and PE) compared with T2D EVs (Fig. 5 and *SI Appendix*, Fig. S3). CH and SM are important membrane components affecting membrane fluidity and lipid raft formation (42), and it has been reported that the presence of SM in PC-based liposomes slows (43), and the addition of CH to synthetic lipid membranes inhibits, IAPP amyloid formation (43, 44). These results support the idea that SM and/or CH in healthy pancreatic EVs may help mediate the inhibitory effect on IAPP amyloid formation. We also found a higher lipid:protein ratio in healthy pancreatic EVs compared with T2D EVs, implying more exposed lipid surfaces in the former (Fig. 5*B*). To pinpoint how healthy EVs bind IAPP on a molecular level, further studies using lipid vesicles of strategic compositions, along with identification of proteins exposed on the EV membrane surfaces, are needed.

Conclusions

Several studies have reported accelerated IAPP amyloid formation in the presence of synthetic vesicles rich in negatively charged lipids. Thus, our finding of healthy pancreatic EVs limiting IAPP amyloid formation is surprising at first glance. However, recent work has shown that IAPP amyloid formation is strongly reduced by the extracellular environment and by plasma membranes of

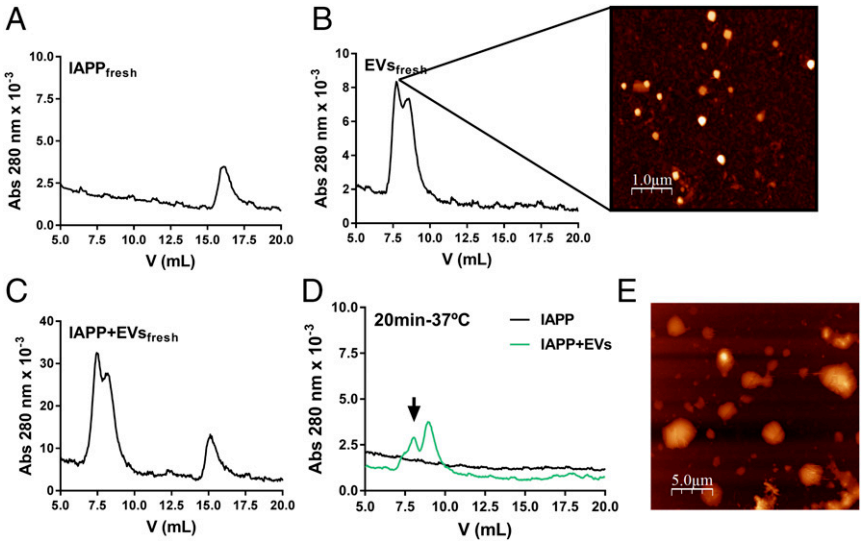

Fig. 4. Assessment of IAPP interaction with healthy pancreatic EVs by SEC and AFM. (*A*) SEC of freshly eluted IAPP (monomers). (*B*) SEC of EVs (elutes in the void), with AFM imaging of the indicated fraction. (*C*) SEC of a mixture of IAPP and EVs without incubation (elutes as monomeric IAPP and EVs in the void, i.e., as a combination of the traces in *A* and *B*). (*D*) SEC of IAPP (which forms amyloids and is filtered away before SEC injection) and a mixture of IAPP and EVs preincubated for 20 min at 37 °C before SEC analysis. The eluate contains no monomeric IAPP; instead, absorption of EVs in void is decreased, which may be explained by the formation of larger particles that are partially filtered away before SEC. The arrow points to reduced absorption of EVs after incubation with IAPP. (*E*) AFM image of an incubated mixture of IAPP and EVs (larger particles than in the AFM image in *B*).

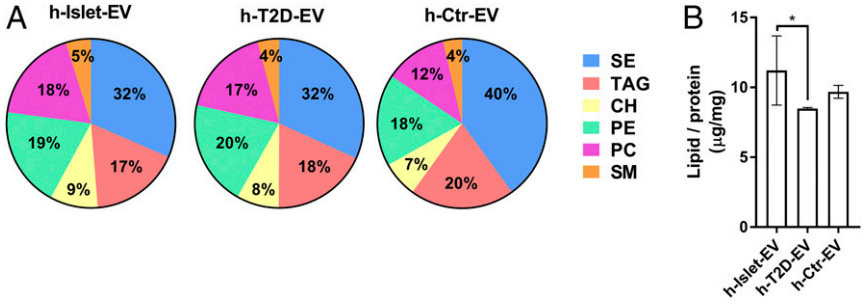

Fig. 5. EV lipid identification. (*A*) Relative mass percentage of the six identified lipid classes found in h-Islet-EVs, h-T2D-EVs, and h-Ctr-EVs, with the total lipid mass detected for each sample set to 100%. (*B*) Ratio of total lipid content to total protein content for each EV population. *Statistical significance: $P < 0.05$.

pancreatic β cells (45). The authors speculated about the presence of particular lipids or proteins in the plasma membranes and/or secreted molecules that mediated this effect. Based on our present results, we propose that secreted EVs from the pancreatic islets used in that study might have mediated the observed inhibitory effects. Of note, we found that the amyloid-reducing effect originated from the EVs themselves, not from any EV-secreted molecule or soluble component in the media, and involved IAPP surface binding and/or internalization. The next step is to identify the molecular mechanisms underlying IAPP amyloid retardation by healthy pancreatic EVs, including the EV lipids and/or proteins that are the key players.

Materials and Methods

Human Pancreatic Islets. Human primary islets isolated from donor pancreases obtained from deceased individuals, with research consent from organ procurement organizations, were purchased from Prodo Laboratories. The use and storage of human islets were conducted in compliance with the Declaration of Helsinki and International Council for Harmonisation of Technical Requirements for Pharmaceuticals for Human Use Good Clinical Practice guidelines, and was approved by an independent Regional Ethics Committee. Islets were transported in PIM(S) medium (Prodo Laboratories) and then transferred to fresh PIM(S) medium for overnight recovery.

EV Isolation. Human pancreatic islet-derived EVs were isolated from fresh pancreatic islet-conditioned media. Donor information is provided in *SI Appendix*, Table S1. Male and female donors were used for the isolation of healthy EVs; only female donors were available for the isolation of T2D-derived EVs. Conditioned medium isolated after 24 h of culture was used for EV isolation. The conditioned medium was freshly centrifuged at 200 × *g* for 10 min, then at 2,000 × *g* for 10 min, and finally at 4,000 × *g* for 60 min. The supernatant was filtered through a 0.45-μm filter and incubated with ExoQuick-TC reagent (System Biosciences) following the manufacturer's instructions. EVs were then resuspended in PBS and stored at −80 °C in small aliquots. PIM(S) medium was used to extract EVs corresponding to the human serum fraction for use as control EVs (h-Ctr-EV). Islets derived from T2D donors were used to isolate h-T2D-EVs, and islets derived from healthy, nondiabetic donors were used to isolate h-islet-EVs.

EV Characterization. EVs were quantified in terms of total protein and particle concentrations. Total protein content was measured using the Pierce BCA Protein Assay Kit (23225; Thermo Fisher Scientific). Particle concentration and size distribution were measured by NTA using a Nanosight LM10 instrument (Malvern Instruments). EVs were diluted in PBS to fit into the resolution window of measurement suggested by the instrument manufacturer. Nanosight NTA 3.1 software was used to capture and analyze the particles. The ζ potential was measured by dynamic light scattering at 25 °C in TBS (Zetasizer Nano ZS; Malvern Instruments). The pancreatic hormones INS (10-1131-01; Mercodia), C-PEP (10-1141-01; Mercodia), and IAPP (LS-F9686; LifeSpan BioSciences) were quantified by ultrasensitive ELISA following the manufacturer's instructions.

Proteins/Peptides. IAPP, obtained from Calbiochem (05-23-2540), was treated with hexafluoroisopropanol (105228; Sigma-Aldrich) before use to dissolve any preexisting aggregates. Purification of α-synuclein was done as described previously (46). Before use, the protein was freeze-dried and dissolved in the appropriate buffer, followed by filtration through a 0.2-μm filter.

Amyloid Formation Assay. IAPP amyloid formation was monitored in a 1-cm cuvette using a Cary Eclipse spectrophotometer (with a magnetic stirrer bar). IAPP aggregation was initiated by pipetting IAPP (2.5 mM stock in hexafluoroisopropanol) into a reaction buffer composed of 10 μM ThT (T3516; Sigma-Aldrich) in TBS (0.05 M Tris·HCl buffer pH 7.6 with 0.15 M NaCl; 93318, Sigma-Aldrich) for a final concentration of 4 μM. The fluorescence signal was recorded every 30 s at 37 °C. α-synuclein amyloid formation reactions were conducted in a plate reader (FLUOstar Optima; BMG Labtech) in TBS buffer in the presence of 20 μM ThT at 37 °C with agitation and a 2-mm glass bead in each well for a final concentration of 70 μM. Samples were typically incubated for 80 h, and fluorescence was measured every 20 min. For both protein plate reader and cuvette experiments, ThT was excited at 440 nm, and emission was recorded at 480 nm. EV supplementation was dosed in μg/mL of total protein and freshly incubated with the peptides. EV-free solution was used as control, using an Amicon Ultra-15 centrifugal filter unit with a membrane of nominal molecular weight limit of 100 kDa. BSA (Sigma-Aldrich) served as a protein control.

TEM. For TEM analysis, 10-μL samples from the fibrillation studies were applied to Formvar-coated 200-mesh size copper grids, incubated for 5 min, washed with Milli-Q water, and stained with 1% uranyl acetate. The grids were examined with a Zeiss LEO 912 Omega transmission electron microscope operating at 120 kV, and images were captured by an Olympus Veleta CCD camera.

SEC. Freshly mixed and incubated samples of 10 μM IAPP with or without 62.5 μg/mL EVs (same ratio as used for the aggregations) were loaded on a Superdex 75 10/300 GL column connected to a Äkta Purifier chromatography system (GE Healthcare) using TBS buffer as eluent and operated at 10 °C. Elution was followed by measurement of absorbance at 280 nm, and 1-mL fractions were collected for AFM analysis.

AFM. Aggregated samples were diluted in Milli-Q water (10–20 times) and deposited on freshly cleaved mica. After 10 min, the mica was rinsed with filtered Milli-Q water and dried under a gentle nitrogen stream. Images were recorded on an NTEGRA Prima setup (NT-MDT) using a gold-coated single-crystal silicon cantilever (NSG01, spring constant of ∼5.1 N/m; NT-MDT) and a resonance frequency of ∼180 kHz. The 512-pixel images were acquired at a 0.5-Hz scan rate. Images were analyzed using WSxM 5.0 software (47).

Lipid Analysis. Each sample was extracted with a chloroform methanol mixture (2:1, vol/vol). The samples were shaken vigorously and incubated for 20 min at 4 °C. After incubation, water was added, followed by shaking and incubation for 10 min at 4 °C. Phase separation was achieved by centrifugation at 8,000 × *g* for 5 min. The organic layer was recovered, and the aqueous layer was re-extracted with a mixture of chloroform and methanol (2:1, vol/vol), shaken vigorously, and centrifuged at 8,000 × *g* for 5 min. The organic layers were combined, evaporated to dryness under a steam of nitrogen, and reconstituted into a chloroform methanol mix (1:1). The samples were analyzed using a HPLC-CAD system as described previously (48).

Statistical Analysis. A minimum of three independent islet donors were used for the different experiments, with a minimum of two technical replicates per

condition and assay, with the exception of the mass spectrometry analysis, for which samples from one donor per condition was used. Data were statistically analyzed using GraphPad Prism version 6.01. The results were analyzed for normal distribution. Parametric or nonparametric methods were used to assess variances in the data depending on the data normality. Automatic correction for outliers was performed using the ROUT method (Q = 1%). The statistical significance of calculated *P* values is defined in *SI Appendix*, Table S2; *P* values of $\leq$0.05 were considered statistically significant in the analysis of the results. Box-and-whisker plot graphs were used to show the distribution of the observed data variation (displayed as minimum to maximum value together with distribution around the median, i.e., upper and lower quartiles).

ACKNOWLEDGMENTS. We thank the Chalmers Mass Spectrometry Infrastructure for data acquisition; the Centre for Cellular Imaging at the Sahlgrenska Academy, University of Gothenburg, for use of imaging equipment and staff support; and Eva-Marie Andersson (Cardiovascular and Metabolic Diseases, Innovative Medicines and Early Development Biotech Unit, AstraZeneca, Gothenburg, Sweden) for kind help with human pancreatic islet handling. Funding was provided by the Knut and Alice Wallenberg Foundation, the Swedish Research Council, and the Chalmers Foundation. D.R. is funded by the People Program (Marie Curie Actions) of the European Union's Seventh Framework Program under REA Grant agreement 607842. N.H. is funded by the AstraZeneca postdoctoral program.

1. World Health Organization (2015) *Global Report on Diabetes* (World Health Organization, Geneva).
2. Knowles TP, Vendruscolo M, Dobson CM (2014) The amyloid state and its association with protein misfolding diseases. *Nat Rev Mol Cell Biol* 15:384–396.
3. Brender JR, Salamekh S, Ramamoorthy A (2012) Membrane disruption and early events in the aggregation of the diabetes-related peptide IAPP from a molecular perspective. *Acc Chem Res* 45:454–462.
4. DeToma AS, Salamekh S, Ramamoorthy A, Lim MH (2012) Misfolded proteins in Alzheimer's disease and type II diabetes. *Chem Soc Rev* 41:608–621.
5. Kotler SA, Walsh P, Brender JR, Ramamoorthy A (2014) Differences between amyloid-β aggregation in solution and on the membrane: Insights into elucidation of the mechanistic details of Alzheimer's disease. *Chem Soc Rev* 43:6692–6700.
6. Patel HR, Pithadia AS, Brender JR, Fierke CA, Ramamoorthy A (2014) In search of aggregation pathways of IAPP and other amyloidogenic proteins: Finding answers through NMR spectroscopy. *J Phys Chem Lett* 5:1864–1870.
7. Cao P, et al. (2013) Islet amyloid: From fundamental biophysics to mechanisms of cytotoxicity. *FEBS Lett* 587:1106–1118.
8. Cao P, Abedini A, Raleigh DP (2013) Aggregation of islet amyloid polypeptide: From physical chemistry to cell biology. *Curr Opin Struct Biol* 23:82–89.
9. Westermark GT, Gebre-Medhin S, Steiner DF, Westermark P (2000) Islet amyloid development in a mouse strain lacking endogenous islet amyloid polypeptide (IAPP) but expressing human IAPP. *Mol Med* 6:998–1007.
10. Matveyenko AV, Butler PC (2008) Relationship between beta-cell mass and diabetes onset. *Diabetes Obes Metab* 10:23–31.
11. Meier JJ, Bonadonna RC (2013) Role of reduced β-cell mass versus impaired β-cell function in the pathogenesis of type 2 diabetes. *Diabetes Care* 36:S113–S119.
12. Suckale J, Solimena M (2010) The insulin secretory granule as a signaling hub. *Trends Endocrinol Metab* 21:599–609.
13. Jaikaran ET, Nilsson MR, Clark A (2004) Pancreatic beta-cell granule peptides form heteromolecular complexes which inhibit islet amyloid polypeptide fibril formation. *Biochem J* 377:709–716.
14. Marzban L, et al. (2006) Impaired NH2-terminal processing of human pro-islet amyloid polypeptide by the prohormone convertase PC2 leads to amyloid formation and cell death. *Diabetes* 55:2192–2201.
15. EL Andaloussi S, Mäger I, Breakefield XO, Wood MJ (2013) Extracellular vesicles: Biology and emerging therapeutic opportunities. *Nat Rev Drug Discov* 12:347–357.
16. Simons M, Raposo G (2009) Exosomes: Vesicular carriers for intercellular communication. *Curr Opin Cell Biol* 21:575–581.
17. Cocucci E, Meldolesi J (2015) Ectosomes and exosomes: Shedding the confusion between extracellular vesicles. *Trends Cell Biol* 25:364–372.
18. Sarko DK, McKinney CE (2017) Exosomes: Origins and therapeutic potential for neurodegenerative disease. *Front Neurosci* 11:82.
19. Barile L, Vassalli G (2017) Exosomes: Therapy delivery tools and biomarkers of diseases. *Pharmacol Ther* 174:63–78.
20. Huang-Doran I, Zhang CY, Vidal-Puig A (2017) Extracellular vesicles: Novel mediators of cell communication in metabolic disease. *Trends Endocrinol Metab* 28:3–18.
21. Lakhter AJ, Sims EK (2015) Minireview: Emerging roles for extracellular vesicles in diabetes and related metabolic disorders. *Mol Endocrinol* 29:1535–1548.
22. Koumoto Y, et al. (1996) Isolation and characterization of a cDNA encoding mitochondrial chaperonin 10 from *Arabidopsis thaliana* by functional complementation of an *Escherichia coli* groES mutant. *Plant J* 10:1119–1125.
23. Bashratyan R, Sheng H, Regn D, Rahman MJ, Dai YD (2013) Insulinoma-released exosomes activate autoreactive marginal zone-like B cells that expand endogenously in prediabetic NOD mice. *Eur J Immunol* 43:2588–2597.
24. Javeed N, et al. (2015) Pancreatic cancer-derived exosomes cause paraneoplastic beta-cell dysfunction. *Clin Cancer Res* 21:17221733, and erratum (2015) 21:4495.
25. Figliolini F, et al. (2014) Isolation, characterization and potential role in beta cell-endothelium cross-talk of extracellular vesicles released from human pancreatic islets. *PLoS One* 9:e102521.
26. Grey M, et al. (2015) Acceleration of α-synuclein aggregation by exosomes. *J Biol Chem* 290:2969–2982.
27. Yuyama K, Sun H, Mitsutake S, Igarashi Y (2012) Sphingolipid-modulated exosome secretion promotes clearance of amyloid-β by microglia. *J Biol Chem* 287:10977–10989.
28. Ngolab J, et al. (2017) Brain-derived exosomes from dementia with Lewy bodies propagate α-synuclein pathology. *Acta Neuropathol Commun* 5:46.
29. Stuendl A, et al. (2016) Induction of α-synuclein aggregate formation by CSF exosomes from patients with Parkinson's disease and dementia with Lewy bodies. *Brain* 139:481–494.
30. Wang H, Cao P, Raleigh DP (2013) Amyloid formation in heterogeneous environments: Islet amyloid polypeptide glycosaminoglycan interactions. *J Mol Biol* 425:492–505.
31. Cao P, et al. (2013) Islet amyloid polypeptide toxicity and membrane interactions. *Proc Natl Acad Sci USA* 110:19279–19284.
32. Seeliger J, et al. (2012) Cross-amyloid interaction of Aβ and IAPP at lipid membranes. *Angew Chem Int Ed Engl* 51:679–683.
33. Jones AG, Hattersley AT (2013) The clinical utility of C-peptide measurement in the care of patients with diabetes. *Diabet Med* 30:803–817.
34. Naiki H, Higuchi K, Hosokawa M, Takeda T (1989) Fluorometric determination of amyloid fibrils in vitro using the fluorescent dye, thioflavin T1. *Anal Biochem* 177:244–249.
35. Xue C, Lin TY, Chang D, Guo Z (2017) Thioflavin T as an amyloid dye: Fibril quantification, optimal concentration and effect on aggregation. *R Soc Open Sci* 4:160696.
36. Uversky VN (2007) Neuropathology, biochemistry, and biophysics of alpha-synuclein aggregation. *J Neurochem* 103:17–37.
37. Spillantini MG, et al. (1997) Alpha-synuclein in Lewy bodies. *Nature* 388:839–840.
38. Polymeropoulos MH, et al. (1997) Mutation in the alpha-synuclein gene identified in families with Parkinson's disease. *Science* 276:2045–2047.
39. Steneberg P, et al. (2013) The type 2 diabetes-associated gene ide is required for insulin secretion and suppression of α-synuclein levels in β-cells. *Diabetes* 62:2004–2014.
40. Horvath I, Wittung-Stafshede P (2016) Cross-talk between amyloidogenic proteins in type-2 diabetes and Parkinson's disease. *Proc Natl Acad Sci USA* 113:12473–12477.
41. Kiskis J, Horvath I, Wittung-Stafshede P, Rocha S (2017) Unraveling amyloid formation paths of Parkinson's disease protein α-synuclein triggered by anionic vesicles. *Q Rev Biophys* 50:1–9.
42. Pike LJ (2003) Lipid rafts: Bringing order to chaos. *J Lipid Res* 44:655–667.
43. Zhang X, St Clair JR, London E, Raleigh DP (2017) Islet amyloid polypeptide membrane interactions: Effects of membrane composition. *Biochemistry* 56:376–390.
44. Cho WJ, Trikha S, Jeremic AM (2009) Cholesterol regulates assembly of human islet amyloid polypeptide on model membranes. *J Mol Biol* 393:765–775.
45. Schlamadinger DE, Miranker AD (2014) Fiber-dependent and -independent toxicity of islet amyloid polypeptide. *Biophys J* 107:2559–2566.
46. Chorell E, et al. (2015) Bacterial chaperones CsgE and CsgC differentially modulate human α-synuclein amyloid formation via transient contacts. *PLoS One* 10:e0140194.
47. Horcas I, et al. (2007) WSXM: A software for scanning probe microscopy and a tool for nanotechnology. *Rev Sci Instrum* 78:013705.
48. Khoomrung S, et al. (2013) Rapid quantification of yeast lipid using microwave-assisted total lipid extraction and HPLC-CAD. *Anal Chem* 85:4912–4919.